Journal of Quantitative Spectroscopy & Radiative Transfer 113 (2012) 67–74

Contents lists available at SciVerse ScienceDirect

Journal of Quantitative Spectroscopy & Radiative Transfer

journal homepage: www.elsevier.com/locate/jqsrt

Einstein A coefficients and absolute line intensities for the $E^2\Pi$–$X^2\Sigma^+$ transition of CaH

Gang Li [a,*], Jeremy J. Harrison [a], Ram S. Ram [a,b], Colin M. Western [c], Peter F. Bernath [a,1]

[a] Department of Chemistry, University of York, Heslington, York YO10 5DD, UK
[b] Department of Chemistry, University of Arizona, Tucson, AZ 85721, USA
[c] School of Chemistry, University of Bristol, Bristol BS8 1TS, UK

ARTICLE INFO

Article history:
Received 27 July 2011
Accepted 12 September 2011
Available online 19 September 2011

Keywords:
Calcium monohydride
Hönl–London factors
Einstein A coefficient
Line intensity calculation
Astrophysical molecules

ABSTRACT

Einstein A coefficients and absolute line intensities have been calculated for the $E^2\Pi$–$X^2\Sigma^+$ transition of CaH. Using wavefunctions derived from the Rydberg–Klein–Rees (RKR) method and electronic transition dipole moment functions obtained from high-level ab initio calculations, rotationless transition dipole moment matrix elements have been calculated for all 10 bands involving $v'=0,1$ of the $E^2\Pi$ state and $v''=0,1,2,3,4$ of the $X^2\Sigma$ state. The rotational line strength factors (Hönl–London factors) are derived for the intermediate coupling case between Hund's case (a) and (b) for the $E^2\Pi$–$X^2\Sigma^+$ transition. The computed transition dipole moments and the spectroscopic constants from a recent study [Ram et al., Journal of Molecular Spectroscopy 2011;266:86–91] have been combined to generate line lists containing Einstein A coefficients and absolute line intensities for 10 bands of the $E^2\Pi$–$X^2\Sigma^+$ transition of CaH for J-values up to 50.5. The absolute line intensities have been used to determine a rotational temperature of 778 ± 3 °C for the CaH sample in the recent study.

1. Introduction

CaH is an important molecule in astrophysics, having been identified in the spectra of sunspots [1,2] and cool brown dwarfs [3,4] through the observation of bands belonging to the $A^2\Pi$–$X^2\Sigma^+$ and $B^2\Sigma^+$–$X^2\Sigma^+$ transitions. The CaH bands are particularly strong in M dwarfs and are used to identify M [5] and L [6,7] type subdwarfs in which metal hydrides are enhanced relative to metal oxides such as TiO. Subdwarfs are metal-poor objects and have very low abundances of heavy elements compared to normal stars like the Sun. The observation of metal hydrides and oxides is, therefore, used as a tool to monitor temperature and composition of the atmospheres of these objects.

As the number of new classes of stellar objects has grown [8–10], the understanding of their atmospheres, evolution, and spectral characteristics remains far from complete. Considerable attempts have been made to develop models to determine their atmospheric parameters such as chemical composition, pressure, surface gravity and temperature. Opacities for the molecular species found in the atmospheres of these objects are needed to achieve this goal. However, complete molecular opacity data for many species found in these atmospheres are still lacking, limiting the development of adequate atmospheric models for cool stars and brown dwarfs.

Among the hydride molecules, molecular opacities have been calculated for the $A^6\Sigma^+$–$X^6\Sigma^+$ transition of CrH [11], the $F^4\Delta$–$X^4\Delta$ transition of FeH [12], the $A^4\Phi$–$X^4\Phi$ transition of TiH [13], and the $A^2\Pi$–$X^2\Sigma^+$ and $B^2\Sigma^+$–$X^2\Sigma^+$ transitions of MgH [14]. In a more recent study, Hargreaves et al. [15] have created a line list at 2200 K for the near-infrared $E^4\Pi$–$A^4\Pi$ and $E^4\Pi$–$X^4\Delta$ transitions of FeH based on laboratory spectra and an ab initio calculation of the band strengths. For CaH, Weck et al. [16] have performed theoretical calculations on the rovibrationally-resolved transitions involving the $A^2\Pi$, $B^2\Sigma^+$ and $E^2\Pi$ excited

* Corresponding author.
E-mail address: gl525@york.ac.uk (G. Li).
[1] Present address: Department of Chemistry, Old Dominion University, Norfolk, VA 23529, USA.

0022-4073/$ - see front matter © 2011 Elsevier Ltd. All rights reserved.
doi:10.1016/j.jqsrt.2011.09.010

states and the $X^2\Sigma^+$ ground states. Their results were in good agreement with the available theoretical and experimental data for the vibrational energy levels and band oscillator strengths. Since the $A^2\Pi$ and $B^2\Sigma^+$ states of CaH are affected by strong interactions between the two states and some other close-lying electronic states, a qualitative fit of the observed transitions is still lacking. A deperturbation analysis of the two transitions is therefore necessary in order to obtain a complete set of spectroscopic constants, including the interaction parameters. Work in this direction is currently being undertaken and the results will enable the calculation of molecular opacities for the $A^2\Pi$–$X^2\Sigma^+$ and $B^2\Sigma^+$–$X^2\Sigma^+$ transitions of CaH using high-resolution experimental data.

Recently we have completed a high resolution analysis of the $E^2\Pi$–$X^2\Sigma^+$ transition of CaH [17] observed in the 20 100–20 700 cm^{-1} spectral region. The spectra were recorded using a Bruker IFS 120 HR Fourier transform spectrometer, and a rotational analysis of the 0–0 and 1–1 bands was carried out in order to obtain an improved set of spectroscopic parameters for the $E^2\Pi$ and $X^2\Sigma^+$ states [17]. These results, combined with the transition dipole moment function of the $E^2\Pi$–$X^2\Sigma^+$ transition determined by Weck et al. [16], have enabled the calculation of Einstein A coefficients and absolute line intensities using the computer programs LEVEL [18] and PGOPHER (version 7.1.108) [19]. Line lists and Einstein A coefficients for different bands of the $E^2\Pi$–$X^2\Sigma^+$ transition have been generated. A summary of the theoretical approach applied, and the results of our calculations will be presented.

2. Methodology

The knowledge of absolute line intensities and Einstein A coefficients of molecular species is of fundamental importance with applications in areas such as astrophysics and atmospheric science [20]. While Einstein A coefficients can be obtained indirectly by measurements of radiative lifetimes, experimental measurements of absolute line intensities require specific experimental conditions which are difficult to obtain for many high temperature molecular species. The rapid increase in computing power and the recent developments in quantum chemistry have made it possible to compute these data, in addition to making experimental measurements. The use of semi-empirical methods that combine the best available experimental and theoretical data can provide the desired information for important molecular species.

Theoretically, the eigenvalues $E_{v,J}$ and eigenfunctions $\psi_{v,J}(r)$ for a diatomic molecule with the potential $V_J(r)$ can be determined by solving the one-dimensional Schrödinger equation. Methods for determining the potential $V_J(r)$ include the RKR (Rydberg–Klein–Rees) method [21], or ab initio calculations. Line intensities for an electronic transition of a diatomic molecule are proportional to the square of the appropriate transition dipole moment matrix element, $\langle \psi_{v'J'}(r)|\Re_e(r)|\psi_{v''J''}(r)\rangle$, where $\Re_e(r)$ is the electronic transition dipole moment. Given the electronic wavefunction, $\psi_{el}(r)$, as a function of internuclear distance, $\Re_e(r)$ can be calculated *ab initio*,

$$\Re_e(r) = \langle \psi'_{el}(r)|\boldsymbol{\mu}(r)|\psi''_{el}(r)\rangle \tag{1}$$

where $\boldsymbol{\mu}(r)$ is the electric dipole moment operator.

The calculation of transition dipole moment matrix elements of the form $\langle \psi_{v'J'}(r)|\Re_e(r)|\psi_{v''J''}(r)\rangle$ is rather involved. However, we have shown in a previous study on HCl [22] that Le Roy's LEVEL program can significantly simplify this procedure and produce transition dipole moment matrix elements with sufficient accuracy for many purposes. Once transition dipole moment matrix elements are extracted from LEVEL, Einstein A coefficients can be calculated with the aid of the PGOPHER program [19] by the relation [23]

$$A_{J'\to J''} = 3.13618932\times10^{-7}\nu^3\frac{\mathcal{S}}{2J'+1}\left|\langle\psi_{v'J'}|\Re_e(r)|\psi_{v''J''}\rangle\right|^2 \tag{2}$$

where $A_{J'\to J''}$ has the units of s^{-1}, ν is the transition wavenumber (cm^{-1}), $\mathcal{S}$ is the rotational line strength factor (Hönl–London factor) which will be discussed in detail later, and $\Re_e$ is the electronic transition dipole moment in debye.

2.1. Hönl–London factors

In general, the line strength, S, for the one-photon electric-dipole-allowed aJ'–bJ'' transition of a diatomic molecule is given by the integral [23]

$$S_{aJ',bJ''} = \sum\nolimits_{p,M',M''}\left|\langle\Psi_{aJ'M'}|T^1_p(\mu)|\Psi_{bJ''M''}\rangle\right|^2 \tag{3}$$

where $\Psi_{aJ'M'}$ and $\Psi_{bJ''M''}$ are the wavefunctions for the magnetic substates of the upper and lower states, respectively, J' and J'' are the total angular momenta, M' and M'' their associated components (in a space-fixed coordinate system), a and b any other necessary quantum numbers, and T^1_p (μ) are the spherical tensor components (in a space-fixed coordinate system) of the transition dipole moment operator.

In order to derive expressions for the line strength, $T^1_p(\mu)$ must be expressed in terms of the molecule-fixed components T^1_q using Wigner $\mathfrak{D}$ matrices [24]

$$T^1_p(\mu) = \sum_q \mathfrak{D}^1_{pq}(\omega)^* T^1_q(\mu) \tag{4}$$

Using case (a) basis functions of the form $|\eta\Lambda;v;S\Sigma;J\Omega M\rangle$ (i.e., a non-parity basis set; refer to Ref. [24] for definitions of the quantum numbers), assuming the radiation is isotropic, and using the Wigner–Eckart theorem, S^{basis} can be written as [24]:

$$\begin{aligned}
S^{basis}_{\eta'\Lambda'v'S'\Sigma'J'\Omega',\eta''\Lambda''v''S''\Sigma''J''\Omega''} &= 3\sum\nolimits_{M',M''}\left|\langle\eta'\Lambda';v';S'\Sigma';J'\Omega'M'|T^1_{p=0}(\mu)|\eta''\Lambda'';\right.\\
&\quad \left.v'';S''\Sigma'';J''\Omega''M''\rangle\right|^2\\
&= 3\sum\nolimits_{M'M''}\left|\sum_q\langle\eta'\Lambda';v';S'\Sigma';J'\Omega'M'|\mathfrak{D}^1_{0q}(\omega)^*T^1_q(\mu)|\eta''\Lambda'';\right.\\
&\quad \left.v'';S''\Sigma'';J''\Omega''M''\rangle\right|^2\\
&= 3\sum\nolimits_{M'M''}\left|\sum_q\langle\eta'\Lambda^{s'}|T^1_q(\mu)|\eta''\Lambda^{s''}\rangle\langle S'\Sigma'|S''\Sigma''\rangle\right.
\end{aligned}$$

$$\times \langle v'|v''\rangle \langle J'\Omega'M'|\mathfrak{D}^1_{0q}(\omega)^*|J''\Omega''M''\rangle\Big|^2$$

$$= 3\delta_{S'S''}\delta_{\Sigma'\Sigma''}q_{v'v''}\sum_{M'M''}\Big|\sum_q(-1)^{J'-M'}\begin{pmatrix} J' & 1 & J'' \\ -M' & 0 & M''\end{pmatrix}$$

$$\times \langle J'\Omega'\|\mathfrak{D}^1_q(\omega)^*\|J''\Omega''\rangle \langle \eta'\Lambda^{s'}|T^1_q(\mu)|\eta''\Lambda^{s''}\rangle\Big|^2$$

$$= \delta_{S'S''}\delta_{\Sigma'\Sigma''}q_{v'v''}\Big|\sum_q(-1)^{J'-\Omega'}\begin{pmatrix} J' & 1 & J'' \\ -\Omega' & q & \Omega''\end{pmatrix}$$

$$\times\sqrt{(2J'+1)(2J''+1)}\langle \eta'\Lambda^{s'}|T^1_q(\mu)|\eta''\Lambda^{s''}\rangle\Big|^2$$

$$= \delta_{S'S''}\delta_{\Sigma'\Sigma''}q_{v'v''}|\mathfrak{R}_e|^2\mathcal{S}_{J'\Omega'J''\Omega''} \quad (5)$$

where $|\mathfrak{R}_e|^2 = |\langle \eta'\Lambda^{s'}|T^1_{\Lambda'-\Lambda''}(\mu)|\eta''\Lambda^{s''}\rangle|^2$ and

$$\mathcal{S}_{J'\Omega'J''\Omega''} = (2J'+1)(2J''+1)\begin{pmatrix} J' & 1 & J'' \\ -\Omega' & \Omega'-\Omega'' & \Omega''\end{pmatrix}^2$$

In this definition, $q_{v'v''}$ is the Franck–Condon factor, $\mathfrak{R}_e$ the electronic transition dipole moment of the molecule, and $\mathcal{S}_{J'\Omega'J''\Omega''}$ the (non-parity) Hönl–London factors (HLFs). The derivation of Eq. (5) makes use of the Franck–Condon principle.

The HLFs for singlet–singlet transitions were originally derived by Hönl and London in 1925 [25]. Analytical formulae of HLFs for higher multiplicity transitions have subsequently been derived during the last century [26–35]. Generally published formulae agree with respect to the relative intensities within a band, however there are often discrepancies by a factor of two or more for the absolute intensities for certain types of transitions. Some of the ambiguities regarding HLFs in the literature were summarized by Hansson and Watson [35] in 2005 for singlet-singlet transitions. Their derivation also showed that the use of parity basis functions introduces an additional factor of two in absolute intensities for the perpendicular transitions $^1\Pi$–$^1\Sigma$ and $^1\Sigma$–$^1\Pi$. For all other singlet-singlet transitions, the use of parity basis functions, as in Eq. (6), produces the same expressions for HLFs due to the symmetry relations between the matrix elements

$$|\eta^{2S+1}|\Lambda|_\Omega vJMpar = \pm 1\rangle = \frac{1}{\sqrt{2}}\Big\{|\eta\Lambda^s;v;S\Sigma;J\Omega M\rangle \pm (-1)^{J-S+s}|\eta-\Lambda^s;v;S-\Sigma;J-\Omega M\rangle\Big\} \quad (6)$$

Hansson and Watson's conclusions for perpendicular $^1\Pi$–$^1\Sigma$ and $^1\Sigma$–$^1\Pi$ transitions can be extended to higher multiplicity even-electron Π–Σ and Σ–Π transitions. In such cases, the associated basis function for the $\Sigma=0$ component of a Σ state is no longer written as a linear combination, but as a single function of the form

$$|\eta^{2S+1}\Sigma^{(s)}_0 vJMpar = J-S+s\rangle = |\eta\Lambda=0^{(s)};v;S\Sigma=0;J\Omega=0M\rangle \quad (7)$$

(For odd-electron systems, all wavefunctions are of the form given in Eq. (6)). It is obvious that any Π–Σ/Σ–Π matrix elements involving the basis function in Eq. (7) must be a factor of two higher than the corresponding matrix element derived in a non-parity basis set. General expressions for HLFs in a case (a) parity basis set ($\mathcal{S}_{J'\Omega'par'J''\Omega''par''}$) are given in Table 1. Note that for the purposes of this table we define $\Lambda\geq 0$. Furthermore, values of Ω must satisfy the requirement $\Delta\Sigma=0$. The entries in Table 1 of Hansson and Watson [35] can be viewed as a special case of those in the present Table 1, with $\Omega=\Lambda$ ($\Sigma=0$ for singlet states).

Note that the total line strength calculated in a basis set with defined parity, $S^{basis}_{\eta'\Lambda'v'S'\Sigma'J'\Omega'par',\eta''\Lambda''v''S''\Sigma''J''\Omega''par''}$, will differ from Eq. (5) when w' or w'' equals 2. The (parity) HLFs, $\mathcal{S}_{J'\Omega'par'J''\Omega''par''}$, in Table 1 reduce to the (non-parity) HLFs, $\mathcal{S}_{J'\Omega'J''\Omega''}$, by setting $w'=w''=1$. Furthermore, it can be shown that the normal "sum rule" [33–35] for HLFs still applies, where the sum is taken over all possible spin-components and Λ-doublets,

$$\sum\mathcal{S}_{J'\Omega'J''\Omega''} = \sum\mathcal{S}_{J'\Omega'par'J''\Omega''par''} = (2-\delta_{\Lambda'0}\delta_{\Lambda''0})(2S+1)(2J+1) \quad (8)$$

2.2. Calculation of Hönl–London factors for a $^2\Pi$–$^2\Sigma^+$ transition

As we have seen, obtaining analytical formulae for HLFs using Hund's case-(a) basis functions is rather straightforward. However, applying these to real molecules requires more work. The Hamiltonian matrices of the lower and upper states need to be diagonalised to produce wavefunctions which are simply linear combinations of the basis functions. The line strength for a particular rovibronic line can then be computed by transforming the basis-calculated transition dipole moment matrix elements using the coefficients from the diagonalisation, and squaring the result.

For the purpose of validation, we have re-derived analytical HLFs for a $^2\Pi$–$^2\Sigma^+$ transition to compare with the output of PGOPHER; these were first derived by Earls in 1935 [28]. Analytical expressions for the eigenstates of a $^2\Pi$ state intermediate between Hund's cases (a) and (b)

Table 1
$\mathcal{S}_{J'\Omega'par'J''\Omega''par''}$.

Transition	P	Q	R
$\Delta\Lambda=0$	$\frac{(J''-\Omega'')(J''+\Omega'')}{J''}$	$\frac{(2J''+1)\Omega''^2}{J''(J''+1)}$	$\frac{(J''+1-\Omega'')(J''+1+\Omega'')}{J''+1}$
$\Delta\Lambda=-1$	$w'\frac{(J''-1+\Omega'')(J''+\Omega'')}{2J''}$	$w'\frac{(2J''+1)(J''+\Omega'')(J''+1-\Omega'')}{2J''(J''+1)}$	$w'\frac{(J''+1-\Omega'')(J''+2-\Omega'')}{2(J''+1)}$
$\Delta\Lambda=+1$	$w''\frac{(J''-1-\Omega'')(J''-\Omega'')}{2J''}$	$w''\frac{(2J''+1)(J''-\Omega'')(J''+1+\Omega'')}{2J''(J''+1)}$	$w''\frac{(J''+1+\Omega'')(J''+2+\Omega'')}{2(J''+1)}$

where

$$w' = 1+\delta_{\Lambda'0}\delta_{\Sigma'0}$$
$$w'' = 1+\delta_{\Lambda''0}\delta_{\Sigma''0}$$

Table 2
General HLF expressions for a $^2\Pi$–$^2\Sigma^+$ transition in which the $^2\Pi$ state is intermediate between Hund's cases (a) and (b). Refer to text for further details.

$^2\Pi$ (upper)	$^2\Sigma^+$ (lower)	$\mathcal{S}_{J'\Omega' par' J''\Omega'' par''}$ [a]
F_1	F_1	$(2J'+1)(2J''+1)\left\{\beta_J^2\begin{pmatrix} J' & 1 & J'' \\ -\frac{3}{2} & 1 & \frac{1}{2}\end{pmatrix}^2+\alpha_J^2\begin{pmatrix} J' & 1 & J'' \\ -\frac{1}{2} & 1 & -\frac{1}{2}\end{pmatrix}^2-2\alpha_J^2\beta_J^2\begin{pmatrix} J' & 1 & J'' \\ -\frac{3}{2} & 1 & \frac{1}{2}\end{pmatrix}\begin{pmatrix} J' & 1 & J'' \\ -\frac{1}{2} & 1 & -\frac{1}{2}\end{pmatrix}\right\}$
F_1	F_2	$(2J'+1)(2J''+1)\left\{\beta_J^2\begin{pmatrix} J' & 1 & J'' \\ -\frac{3}{2} & 1 & \frac{1}{2}\end{pmatrix}^2+\alpha_J^2\begin{pmatrix} J' & 1 & J'' \\ -\frac{1}{2} & 1 & -\frac{1}{2}\end{pmatrix}^2+2\alpha_J^2\beta_J^2\begin{pmatrix} J' & 1 & J'' \\ -\frac{3}{2} & 1 & \frac{1}{2}\end{pmatrix}\begin{pmatrix} J' & 1 & J'' \\ -\frac{1}{2} & 1 & -\frac{1}{2}\end{pmatrix}\right\}$
F_2	F_1	$(2J'+1)(2J''+1)\left\{\alpha_J^2\begin{pmatrix} J' & 1 & J'' \\ -\frac{3}{2} & 1 & \frac{1}{2}\end{pmatrix}^2+\beta_J^2\begin{pmatrix} J' & 1 & J'' \\ -\frac{1}{2} & 1 & -\frac{1}{2}\end{pmatrix}^2+2\alpha_J^2\beta_J^2\begin{pmatrix} J' & 1 & J'' \\ -\frac{3}{2} & 1 & \frac{1}{2}\end{pmatrix}\begin{pmatrix} J' & 1 & J'' \\ -\frac{1}{2} & 1 & -\frac{1}{2}\end{pmatrix}\right\}$
F_2	F_2	$(2J'+1)(2J''+1)\left\{\alpha_J^2\begin{pmatrix} J' & 1 & J'' \\ -\frac{3}{2} & 1 & \frac{1}{2}\end{pmatrix}^2+\beta_J^2\begin{pmatrix} J' & 1 & J'' \\ -\frac{1}{2} & 1 & -\frac{1}{2}\end{pmatrix}^2-2\alpha_J^2\beta_J^2\begin{pmatrix} J' & 1 & J'' \\ -\frac{3}{2} & 1 & \frac{1}{2}\end{pmatrix}\begin{pmatrix} J' & 1 & J'' \\ -\frac{1}{2} & 1 & -\frac{1}{2}\end{pmatrix}\right\}$
F_1 ($J'=0.5$)[b]	F_1/F_2	$2(2J''+1)\begin{pmatrix} \frac{1}{2} & 1 & J'' \\ -\frac{1}{2} & 1 & -\frac{1}{2}\end{pmatrix}^2$

[a] $\alpha_J=\left[\frac{X_J+(Y-2)}{2X_J}\right]^{1/2}$ and $\beta_J=\left[\frac{X_J-(Y-2)}{2X_J}\right]^{1/2}$.

[b] For the E$^2\Pi$ state of CaH, the special case of $J'=0.5$ corresponds to F_1.

Table 3
Hönl–London Factors for $^2\Pi$–$^2\Sigma^+$ transitions.

$^2\Pi$–$^2\Sigma^+$	$\mathcal{S}_{J'\Omega' par' J''\Omega'' par''}$ [a]
$P_1(J)$	$\frac{(2J-1)^2+(2J-1)X_{J-1}^{-1}(4J^2-4J-7+2Y)}{8J}$
$Q_1(J)$	$\frac{(2J+1)[(4J^2+4J-1)+X_J^{-1}(8J^3+12J^2-2J-7+2Y)}{8J(J+1)}$
$R_1(J)$	$\frac{(2J+3)^2+(2J+3)X_{J+1}^{-1}(4J^2+12J+9-2Y)}{8(J+1)}$
$P_{12}(J)$	$\frac{(2J-1)^2-(2J-1)X_{J-1}^{-1}(4J^2-4J+1-2Y)}{8J}$
$Q_{12}(J)$	$\frac{(2J+1)[(4J^2+4J-1)-X_J^{-1}(8J^3+12J^2-2J+1-2Y)}{8J(J+1)}$
$R_{12}(J)$	$\frac{(2J+3)^2-(2J+3)X_{J+1}^{-1}(4J^2+12J+1+2Y)}{8(J+1)}$
$P_2(J)$	$\frac{(2J-1)^2+(2J-1)X_{J-1}^{-1}(4J^2-4J+1-2Y)}{8J}$
$Q_2(J)$	$\frac{(2J+1)[(4J^2+4J-1)+X_J^{-1}(8J^3+12J^2-2J+1-2Y)}{8J(J+1)}$
$R_2(J)$	$\frac{(2J+3)^2+(2J+3)X_{J+1}^{-1}(4J^2+12J+1+2Y)}{8(J+1)}$
$P_{21}(J)$	$\frac{(2J-1)^2-(2J-1)X_{J-1}^{-1}(4J^2-4J-7+2Y)}{8J}$
$Q_{21}(J)$	$\frac{(2J+1)[(4J^2+4J-1)-X_J^{-1}(8J^3+12J^2-2J-7+2Y)}{8J(J+1)}$
$R_{21}(J)$	$\frac{(2J+3)^2-(2J+3)X_{J+1}^{-1}(4J^2+12J+9-2Y)}{8(J+1)}$
$Q_{12}(0.5)$, $Q_1(0.5)$[b]	$\frac{4}{3}$
$P_{12}(1.5)$, $P_1(1.5)$[b]	$\frac{2}{3}$

[a] $X_J=\left\{(Y-2)^2+4\left[\left(J+\frac{1}{2}\right)^2-1\right]\right\}^{1/2}$; $Y=A/B$.

[b] For the E$^2\Pi$ state of CaH, the special case of $J'=0.5$ corresponds to F_1.

are derived in the Appendix A using a simple version of the N^2 Hamiltonian [24]. $^2\Sigma^+$ eigenstates can be found in various text books, e.g. [23]. General expressions for these HLFs are given in Table 2, with analytical expressions (upon substitution of Wigner 3-j symbols, etc.) for 12 branches of a $^2\Pi$–$^2\Sigma^+$ transitions listed in Table 3. The parity for each entry in Tables 2 and 3 is determined by that of the lower $^2\Sigma^+$ state: for F_1, the parity of each J-level is equated with $(-1)^{J-1/2}$; for F_2, with $(-1)^{J+1/2}$. Upper-state parities must satisfy the relationship $par'par''=-1$.

Using the definitions outlined in this paper, the HLFs derived for a $^2\Pi$–$^2\Sigma$ transition (Table 3) are four times larger than the values calculated by Earls et al. [28]. The outputs of PGOPHER for the HLFs are consistent with the analytical formulae in Table 3, providing confidence in using PGOPHER to calculate Einstein A coefficients and line intensities.

3. Details of the calculations and the results

Potential energy functions, $V_J(r)$, for both the E$^2\Pi$ and X$^2\Sigma^+$ states of CaH were constructed using the purely numerical RKR method [21] with the Kaiser correction [36] and the effective Dunham coefficients from Ram et al. [17]. These RKR potential curves were then employed in the LEVEL program to calculate the wavefunctions, ψ_{vJ}. Note that the current version of LEVEL is limited to singlet-singlet electronic transitions. Therefore, we use LEVEL and the high-level ab initio electronic transition dipole moments, $\Re_e(r)$, from Weck et al. for the E$^2\Pi$–X$^2\Sigma^+$ transition [16], to calculate transition dipole moment matrix elements for $R(0)$ lines of a $^1\Pi$–$^1\Sigma$ transition, i.e. $\langle v'J'_{=1}|\Re_e(r)|v''J''_{=0}\rangle$, for all 10 bands with $v'=0,1$ and $v''=0, 1, 2, 3, 4$; these are listed in Table 4. Considering the minor differences between $\langle v'J'_{=1}|\Re_e(r)|v''J''_{=0}\rangle$ and $\langle v'J'_{=0}|\Re_e(r)|v''J''_{=0}\rangle$, less than 1% in this case, $\langle v'J'_{=1}|\Re_e(r)|v''J''_{=0}\rangle$ was used as the 'rotationless matrix element' in order to avoid Herman–Wallis fitting.

Einstein A coefficients and absolute line intensities for all 10 bands of the E$^2\Pi$–X$^2\Sigma^+$ transition of CaH were calculated using PGOPHER. Firstly, the rovibronic transition wavenumbers were calculated using the spectroscopic constants derived by Shayesteh et al. [37] for $v=0$–4 of the X$^2\Sigma^+$ state and Ram et al. [17] for $v=0$, 1 of the E$^2\Pi$ state. Next, the transition dipole moment matrix elements for $R(0)$ lines of a $^1\Pi$–$^1\Sigma$ transition listed in Table 4 for the 10 bands were inserted into PGOPHER and absolute line intensities calculated.

The absolute line intensities were used to determine the rotational temperature of the CaH sample in the experiments of Ref. [17]. PGOPHER has a useful function to determine the rotational temperature (T_R). T_R was determined as 778 ± 3 °C, which compares well with the

estimated experimental temperature of 780 °C [17]. In the present study, the vibrational temperature, T_V, was set equal to T_R.

Fig. 1 shows the contour fit result using PGOPHER. The unfitted feature marked with a triangle in the residuals is due to a weak argon atomic line. In addition, two lines were locally perturbed and their positions have been marked with asterisks. These two perturbed lines were previously reported in Ref. [17]. The 1–1 band did not fit well due to the presence of perturbations. The $E^2\Pi$ state probably interacts with the $D^2\Sigma^+$ state or the higher vibrational levels of the $B^2\Sigma^+$ state. As reported in Ref. [17], the $D^2\Sigma^+$ state lies only 2132 cm^{-1} above the $E^2\Pi$ state.

Finally, PGOPHER was used to generate a line list (including line positions, Einstein A coefficients and absolute line intensities) for the 10 bands of the $E^2\Pi$–$X^2\Sigma^+$ transition of CaH for J-values up to 50.5. The line positions of the 0–0 band agree well with the experimental values apart from two locally perturbed lines. However, due to the perturbations in the 1–1 band as reported by Ram et al., the line positions have a larger standard deviation of 0.02 cm^{-1} [17]. For the intensities, an overview of the comparison of experimental and simulated spectra for the 0–0 and 1–1 bands of the $E^2\Pi$–$X^2\Sigma^+$ transition of CaH is provided in Fig. 1. Similarly, a comparison for the Q_1 and Q_2 branches is provided in Fig. 2. As shown in Figs. 1 and 2, the simulated spectra agree very well with the experimental spectra.

There are four main sources of error in our calculations:

1) The uncertainty in the ab initio transition dipole moments, which were not discussed in Ref. [16].
2) The error from assuming that transition dipole moment matrix elements for a $^1\Pi$–$^1\Sigma$ transition are the same as the CaH $E^2\Pi$–$X^2\Sigma^+$ transition. At lowest J, the difference is likely to be very small because this is basically equivalent to the validity of the Hund's case (a) basis. Furthermore, as demonstrated in Ref. [22], the errors caused by using wave functions from RKR potentials are small.
3) Uncertainty by not including the rotation–vibration interaction, i.e., Herman–Wallis effect [38] in the calculation of line intensities.
4) Interaction of the $E^2\Pi$ state with a close-lying $^2\Sigma^+$ state. There is another $D^2\Sigma^+$ state lying only 2312 cm^{-1} above $E^2\Pi$ state. Symmetry requires any resulting state mixing to be J-dependent.

Although, the uncertainty arising from source 2, 3, and 4 is hard to evaluate, the overall effect can be estimated by the standard deviation of the intensity fit which is less than 10% for the Q_1, Q_2 branches and 15% for the P_1, P_2 and R_1, R_2 branches.

Table 4
LEVEL outputs for a $^2\Pi$–$^2\Sigma^+$ transition of CaH using RKR potentials and transition dipole moment function from Ref. [16].

$\Delta J(J'')$	v'	v''	A (Einstein)/s^{-1}	$\langle v'j'\|R\|v''j''\rangle$/debye[a]
$R(0)$	0	0	1.04395×10^{6}	0.767167
$R(0)$	0	1	1.58329×10^{3}	−0.032876
$R(0)$	0	2	6.97259×10^{2}	0.024089
$R(0)$	0	3	8.86349×10^{-1}	0.000952
$R(0)$	0	4	7.46177×10^{-3}	−0.000097
$R(0)$	1	0	4.16855×10^{3}	0.044494
$R(0)$	1	1	1.05409×10^{6}	0.774310
$R(0)$	1	2	1.90705×10^{2}	−0.011430
$R(0)$	1	3	2.66231×10^{3}	0.047015
$R(0)$	1	4	5.94906×10^{-2}	−0.000246

[a] Vibronic transition moment input to PGOPHER.

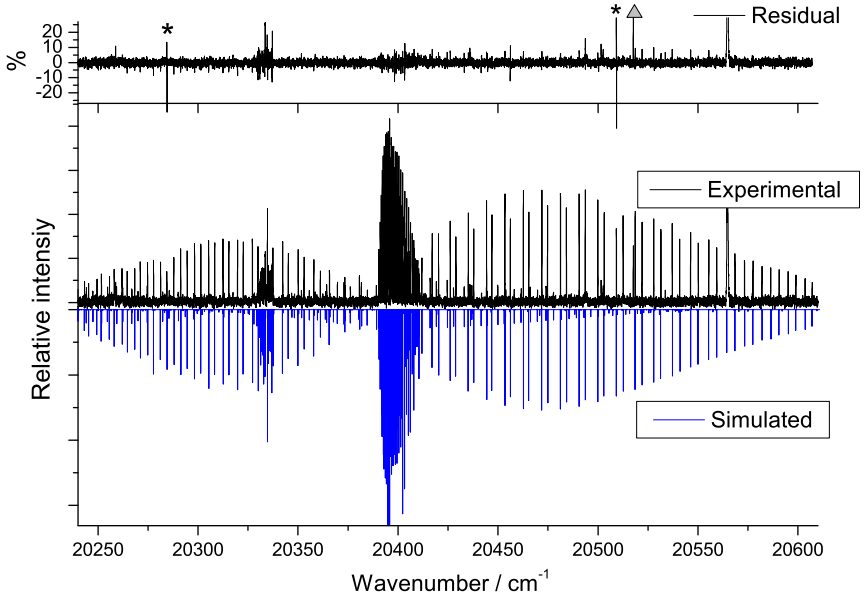

Fig. 1. Overview of experimental (upper curve) and simulated (lower curve) spectra for the 0–0 and 1–1 bands of the $E^2\Pi$–$X^2\Sigma^+$ transition of CaH. In the top panel, the residuals (observed minus calculated spectra) are displayed as a percentage with the largest peak in the experimental spectrum set to 100%. The unfitted features include: a strong argon atomic line around 20565 wavenumber; a weak argon atomic line marked with a triangle in the residuals and two locally perturbed lines marked with asterisks.

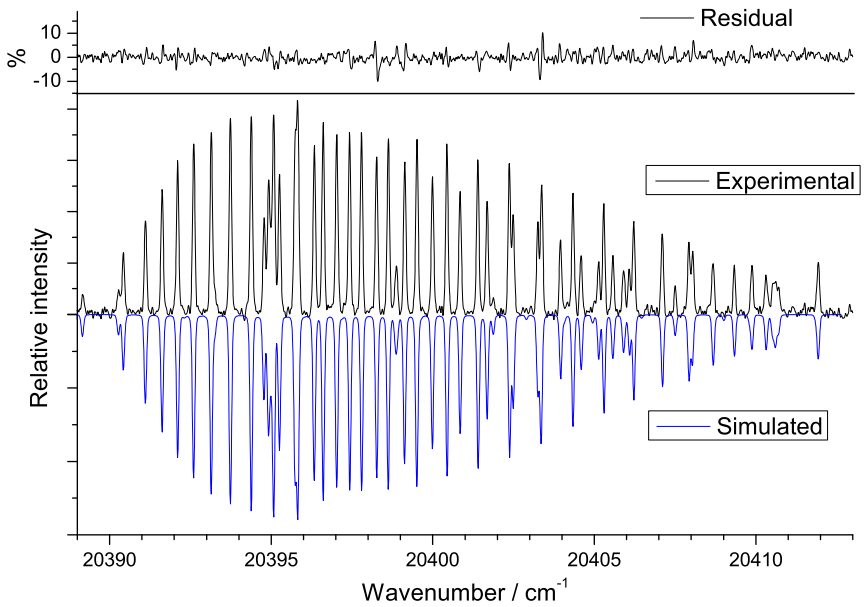

Fig. 2. Experimental (upper) and simulated (lower) spectra of the Q_1 and Q_2 branches of the 0–0 band of the $E^2\Pi$–$X^2\Sigma^+$ transition of CaH. In the top panel, the residuals are displayed as a percentage with the largest peak in the experimental spectrum set to 100%.

Recently, Liu et al. have measured the lifetime of the $A^2\Pi$ state of CaH [39], which allows us to check our Hönl–London factors for a $^2\Pi$–$^2\Sigma^+$ transition. Using the transition dipole moment function for the $A^2\Pi$–$X^2\Sigma^+$ transition of CaH from Weck et al. [16], the transition dipole moment at the ground state equilibrium geometry is 5.694 debye. Since the X and A state potentials are fairly similar, this value seems reasonable. Liu et al. quote a value of 5.655 debye as determined from the lifetime, which is in good agreement with the value derived from Weck et al. A final check was performed by calculating the lifetime using the value 5.694 debye for the transition dipole moment. PGOPHER gives a lifetime around 33 ns for the $A^2\Pi$ state, which is in good agreement with the measured lifetime 33.2 ns [39].

4. Conclusions and future work

Computed transition dipole moments [16] and the spectroscopic constants from a recent study [17] have been used with the PGOPHER program to generate line lists containing Einstein A coefficients and absolute line intensities for 10 bands of the $E^2\Pi$–$X^2\Sigma^+$ transition of CaH for J-values up to 50.5. The line intensities have enabled the determination of a rotational temperature, T_R, of 778 ± 3 °C for the CaH sample in Ref. [17]. The calculated line intensities agree well with experimental values, with a standard deviation of 10% for the Q_1, Q_2 branches and 15% for the P_1, P_2 and R_1, R_2 branches.

Analytical formulae for Hönl–London factors have been derived for a $^2\Pi$–$^2\Sigma^+$ transition using a spherical tensor approach, with the $^2\Pi$ state intermediate between Hund's case (a) and case (b) coupling. Our derived formulae are a factor of 4 larger than those by Earls et al. [28]. A further examination reveals that our derivation agrees with the sum rule in Ref. [34], which has become standard. Our analytical formulae for HLFs in Table 3 agree with values given by PGOPHER for the $^2\Pi$–$^2\Sigma^+$ transition. These HLFs were validated by comparing
the upper-state lifetime calculated by PGOPHER for the $A^2\Pi$–$X^2\Sigma^+$ transition of CaH (using *ab initio* transition dipole moments [16]) with the experimental lifetime [39]; these are in good agreement.

The present study has demonstrated that the use of LEVEL and PGOPHER significantly simplifies the procedure of calculating Einstein A coefficients and absolute line intensities. However, some improvements are still needed. The current version of PGOPHER cannot accept internuclear distance dependent $\mathfrak{R}_e(r)$ to calculate the transition dipole moments. Thus the rotation–vibration interaction, i.e., Herman–Wallis effect [38], was ignored in calculating the line intensities.

Acknowledgement

Support for this work was provided by a Research Project Grant from the Leverhulme Trust, the UK Engineering and Physical Sciences Research Council (EPSRC) and the Wilde Fund of the Chemistry Department at the University of York.

Appendix A.

In the following derivations, all the terms and constants have their usual meaning [24]. In order to determine the eigenstates for a $^2\Pi$ state intermediate between Hund's coupling cases (a) and (b), we use a simple version of the $\mathbf{N}^2$ Hamiltonian incorporating only the following

rotational and spin–orbit terms

$$\mathscr{H}_{\rm rot} = B\mathbf{N}^2 = B(\mathbf{J}-\mathbf{S})^2 \tag{9}$$

$$\mathscr{H}_{\rm SO} = AL_zS_z \tag{10}$$

There are four case-(a) parity basis functions associated with a $^2\Pi$ state

$$|^2\Pi_{3/2}JM\pm\rangle = \frac{1}{\sqrt{2}}\left\{\left|\Lambda=1;S=\frac{1}{2},\Sigma=\frac{1}{2};J,\Omega=\frac{3}{2},M\right\rangle \pm(-1)^{J-1/2}\left|\Lambda=-1;S=\frac{1}{2},\Sigma=-\frac{1}{2};J,\Omega=-\frac{3}{2},M\right\rangle\right\} \tag{11a}$$

$$|^2\Pi_{1/2}JM\pm\rangle = \frac{1}{\sqrt{2}}\left\{\left|\Lambda=1;S=\frac{1}{2},\Sigma=-\frac{1}{2};J,\Omega=\frac{1}{2},M\right\rangle \pm(-1)^{J-1/2}\left|\Lambda=-1;S=\frac{1}{2},\Sigma=\frac{1}{2};J,\Omega=-\frac{1}{2},M\right\rangle\right\} \tag{11b}$$

Using these basis functions and the Hamilton terms in Eqs. (11a) and (11b), the following matrix elements are obtained [24].

Note that the matrix elements are identical for each $\pm$ parity block. Diagonalisation of the matrix in Table 5 provides the following eigenvalues (for $J \geq 1.5$):

$$E(\pm) = B(J+1)^2 \pm \frac{1}{2}\left\{(A-2B)^2+4B^2\left[\left(J+\frac{1}{2}\right)^2-1\right]\right\}^{\frac{1}{2}} = B\left(J+\frac{1}{2}\right)^2 \pm \frac{1}{2}BX_J \tag{12}$$

where

$$X_J = \left\{(Y-2)^2+4\left[\left(J+\frac{1}{2}\right)^2-1\right]\right\}^{1/2}, \quad Y=\frac{A}{B}$$

Note that the + and − signs in Eq. (12) refer to the upper (F_2) and lower (F_1) levels, respectively, and not to the parity. The associated eigenfunctions are:

$$|F_2\pm\rangle = \alpha_J|^2\Pi_{3/2}JM\pm\rangle - \beta_J|^2\Pi_{1/2}JM\pm\rangle \tag{13a}$$

$$|F_1\pm\rangle = \beta_J|^2\Pi_{3/2}JM\pm\rangle + \alpha_J|^2\Pi_{1/2}JM\pm\rangle \tag{13b}$$

where $\alpha_J = [(X_J+(Y-2))/2X_J]^{1/2}$ and $\beta_J = [(X_J-(Y-2))/2X_J]^{1/2}$

In the special case when $J=0.5$, and assuming $A>0$, the eigenvalue and eigenvector is given by

$$E\left(J=\frac{1}{2}\right) = -\frac{A}{2}+2B \tag{14}$$

$$|F_1\pm\rangle = |^2\Pi_{1/2}JM\pm\rangle \tag{15}$$

Table 5
Matrix elements of $\mathscr{H}_{\rm rot}+\mathscr{H}_{\rm SO}$ for a $^2\Pi$ state.

$\mathscr{H}_{\rm rot}+\mathscr{H}_{\rm SO}$	$\lvert^2\Pi_{3/2}JM\pm\rangle$	$\lvert^2\Pi_{1/2}JM\pm\rangle$
$\langle^2\Pi_{3/2}JM\pm\rvert$	$\frac{A}{2}+B\left[\left(J+\frac{1}{2}\right)^2-1\right]$	$-B\left[\left(J+\frac{1}{2}\right)^2-1\right]^{1/2}$
$\langle^2\Pi_{1/2}JM\pm\rvert$	$-B\left[\left(J+\frac{1}{2}\right)^2-1\right]^{1/2}$	$-\frac{A}{2}+B\left[\left(J+\frac{1}{2}\right)^2+1\right]$

Appendix B. Supplementary materials

Supplementary materials associated with this article can be found in the online version at doi:10.1016/j.jqsrt.2011.09.010.

References

[1] Olmsted CM. Sun-spot bands which appear in the spectrum of a calcium arc burning in the presence of hydrogen. Astrophysical Journal 1908;27:66–9.
[2] Eagle A. On the spectra of some of the compounds of the alkaline earths. Astrophysical Journal 1909;30:231–6.
[3] Kirkpatrick JD. New spectral types L and T. Annual Review of Astronomy and Astrophysics 2005;43:195–245.
[4] Burrows A, Hubbard WB, Lunine JI, Liebert J. The theory of brown dwarfs and extrasolar giant planets. Reviews of Modern Physics 2001;73:719–65.
[5] Lepine S, Shara MM, Rich RM. Discovery of an ultracool subdwarf: LSR 1425+7102, the first star with spectral type sdM8.0. Astrophysical Journal 2003;585:L69–72.
[6] Lepine S, Rich RM, Shara MM. LSR 1610-0040: the first early-type L subdwarf. Astrophysical Journal 2003;591:L49–52.
[7] Burgasser AJ, Cruz KL, Kirkpatrick JD. Optical spectroscopy of 2MASS color-selected ultracool subdwarfs. Astrophysical Journal 2007;657:494–510.
[8] Stone RC, Monet DG, Monet AKB, Walker RL, Ables HD, Bird AR, et al. The Flagstaff astrometric scanning transit telescope (FASTT) and star positions determined in the extragalactic reference frame. Astronomical Journal 1996;111:1721–42.
[9] Tinney CG. CCD astrometry of southern very low-mass stars. Monthly Notices of the Royal Astronomical Society 1996;281:644–58.
[10] Mera D, Chabrier G, Baraffe I. Determination of the low-mass star mass function in the galactic disk. Astrophysical Journal 1996;459:L87–90.
[11] Burrows A, Ram RS, Bernath P, Sharp CM, Milsom JA. New CrH opacities for the study of L and brown dwarf atmospheres. Astrophysical Journal 2002;577:986–92.
[12] Dulick M, Bauschlicher CW, Burrows A, Sharp CM, Ram RS, Bernath P. Line intensities and molecular opacities of the FeH $F^4\Delta_i$–$X^4\Delta_i$ transition. Astrophysical Journal 2003;594:651–63.
[13] Burrows A, Dulick M, Bauschlicher CW, Bernath PF, Ram RS, Sharp CM, et al. Spectroscopic constants, abundances, and opacities of the TiH molecule. Astrophysical Journal 2005;624:988–1002.
[14] Weck PF, Schweitzer A, Stancil PC, Hauschildt PH, Kirby K. The molecular continuum opacity of (MgH)-Mg-24 in cool stellar atmospheres. Astrophysical Journal 2003;584:459–64.
[15] Hargreaves RJ, Hinkle KH, Bauschlicher CW, Wende S, Seifahrt A, Bernath PF. High-resolution 1.6 μm spectra of FeH in M and L dwarfs. Astron J 2010;140:919–24.
[16] Weck PF, Stancil PC, Kirby K. Theoretical study of the rovibrationally resolved transitions of CaH. Journal of Chemical Physics 2003;118:9997–10005.
[17] Ram RS, Tereszchuk K, Gordon IE, Walker KA, Bernath PF. Fourier transform emission spectroscopy of the $E^2\Pi$–$X^2\Sigma^+$ transition of CaH and CaD. Journal of Molecular Spectroscopy 2011;266:86–91.
[18] Le Roy RJ. LEVEL 8.0. 2007. p. University of Waterloo Chemical Physics Research Report CP-663, 2007, see 〈http://scienide2.uwaterloo.ca/~rleroy/level/〉.
[19] Western CM. PGOPHER, a Program for Simulating Rotational Structure, C. M. Western, University of Bristol, 〈http://pgopher.chm.bris.ac.uk.〉 7.1.108 ed2010.
[20] Bernath PF. Molecular astronomy of cool stars and sub-stellar objects. International Reviews in Physical Chemistry 2009;28:681–709.
[21] Le Roy RJ. RKR1 2.0, University of Waterloo Chemical Physics Research Report CP-657R, 2004, see 〈http://scienide2.uwaterloo.ca/~rleroy/rkr/〉.
[22] Li G, Gordon IE, Bernath PF, Rothman LS. Direct fit of experimental ro-vibrational intensities to the dipole moment function: Application to HCl. Journal of Quantitative Spectroscopy and Radiative Transfer 2011;112:1543–50.
[23] Bernath PF. Spectra of Atoms and Molecules. second edition, Oxford University Press; 2005 Ed.

[24] Brown JM, Carrington A. Rotational Spectroscopy of Diatomic Molecules. Cambridge, United Kingdom: Cambridge University Press; 2003.
[25] Hönl H, London F. The intensities of the band lines. Zeitschrift Fur Physik 1925;33:803–9.
[26] Hill E, Van Vleck JH. On the quantum mechanics of the rotational distortion of multiplets in molecular spectra. Physical Review 1928;32:250.
[27] Mulliken RS. The interpretation of band spectra. Part IIc. Empirical band types. Reviews of Modern Physics 1931;3:0089–155.
[28] Earls LT. Intensities in $^2\Pi$–$^2\Sigma$ transitions in diatomic molecules. Physical Review 1935;48:423–4.
[29] Herzberg G. Molecular Spectra and Molecular Structure. second edition Malabar, Florida: Krieger Publishing Company; 1950.
[30] Tatum JB. Interpretation of intensities in diatomic molecular spectra. Astrophysical Journal 1967;14:21–56.
[31] Bennett RJM. Hönl–London factors for doublet transitions in diatomic molecules. Monthly Notices of the Royal Astronomical Society 1970;147:35–46.
[32] Whiting EE, Nicholls RW. Reinvestigation of rotational-line intensity factors in diatomic spectra. Astrophysical Journal Supplement Series 1974;27:1–19.
[33] Schadee A. Unique definitions for band strength and electronic-vibrational dipole-moment of diatomic molecular radiative transitions. Journal of Quantitative Spectroscopy & Radiative Transfer 1978;19:451–3.
[34] Whiting EE, Schadee A, Tatum JB, Hougen JT, Nicholls RW. Recommended conventions for defining transition moments and intensity factors in diatomic molecular-spectra. Journal of Molecular Spectroscopy 1980;80:249–56.
[35] Hansson A, Watson JKG. A comment on Hönl–London factors. Journal of Molecular Spectroscopy 2005;233:169–73.
[36] Kaiser EW. Dipole moment and hyperfine parameters of $H^{35}Cl$ and $D^{35}Cl$. The Journal of Chemical Physics 1970;53:1686–703.
[37] Shayesteh A, Walker KA, Gordon I, Appadoo DRT, Bernath PF. New Fourier transform infrared emission spectra of CaH and SrH: combined isotopomer analyses with CaD and SrD. Journal of Molecular Structure 2004;695:23–37.
[38] Herman R, Rothery RW, Rubin RJ. Line intensities in vibration-rotation bands of diatomic molecules. Journal of Molecular Spectroscopy 1958;2:369–86.
[39] Liu M, Pauchard T, Sjödin M, Launila O, van der Meulen P, Berg LE. Time-resolved study of the $A^2\Pi$ state of CaH by laser spectroscopy. Journal of Molecular Spectroscopy 2009;257:105–7.